Long-lived geomagnetic storms and coronal mass ejections

H. Xie,[1,2] N. Gopalswamy,[3] P. K. Manoharan,[4] A. Lara,[5] S. Yashiro,[1,2] and S. Lepri[6]

Received 24 June 2005; revised 17 October 2005; accepted 28 October 2005; published 13 January 2006.

[1] Coronal mass ejections (CMEs) are major solar events that are known to cause large geomagnetic storms ($Dst < -100$ nT). Isolated geomagnetic storms typically have a main phase of 3–12 hours and a recovery phase of around 1 day. However, there are some storms with main and recovery phases exceeding ∼3 days. We trace the origin of these long-lived geomagnetic storms (LLGMS) to frontside halo CMEs. We studied 37 LLGMS events with $Dst < -100$ nT and the associated CMEs which occurred during 1998–2002. It is found that LLGMS events are caused by (1) successive CMEs, accounting for ∼64.9% (24 of 37); (2) single CMEs, accounting for ∼21.6% (8 of 37); and (3) high-speed streams (HSS) in corotating interaction regions (CIRs) with no related CME, accounting for ∼13.5% (5 of 37). The long duration of the LLGMS events was found to be due to successive CMEs and HSS events; the high intensity of the LLGMS events was related to the interaction of CMEs with other CMEs and HSS events. We find that the duration of LLGMS is well correlated to the number of participating CMEs (correlation coefficient $r = 0.78$). We also find that the intensity of LLGMS has a good correlation with the degree of interaction (the number of CMEs interacting with a HSS event or with themselves) ($r = 0.67$). The role of preconditioning in LLGMS events, where the *Dst* development occurred in multiple steps in the main and recovery phases, has been investigated. It is found that preconditioning does not affect the main phase of the LLGMS events, while it plays an important role during the recovery phase of the LLGMS events.

Citation: Xie, H., N. Gopalswamy, P. K. Manoharan, A. Lara, S. Yashiro, and S. T. Lepri (2006), Long-lived geomagnetic storms and coronal mass ejections, *J. Geophys. Res.*, *111*, A01103, doi:10.1029/2005JA011287.

1. Introduction

[2] Intense geomagnetic storms generally occur when solar wind with intense, long-duration southward interplanetary magnetic field (IMF) impacts Earth's magnetosphere. During geomagnetic storms, southward IMF reconnects with Earth's geomagnetic field at the dayside magnetopause, resulting in a chain of events leading to the dramatic increase of the ring current westward, which induces a magnetic field opposite to the geomagnetic field and causes global depression in the horizontal component (H) of the geomagnetic field. It has been known since the work of *Burton et al.* [1975] that the intensity of geomagnetic storms is proportional to the interplanetary dawn-dusk electric field $E = -V_{sw} \times B_s/c$, where V_{sw} is the solar wind flow speed and B_s is the southward component of the IMF [e.g., *Tsurutani and Gonzalez*, 1997; *Gonzalez et al.*, 1994]. *Burton et al.* [1975] provided a simple formula describing the dependence of the energy injection into the ring current system as a function of the solar wind electric field E, indicating that the duskward E is generally associated with the observed negative *Dst* peak (an index proportional to the kinetic energy of the ring current particles) during the storm. Using an empirical model, *O'Brien and McPherron* [2000] found that this energy injection is proportional to $E - E_c$, where the threshold to the electric field $E_c = 0.49$ mV/m. Large-intensity storms are expected to be a more direct response to the interplanetary conditions, where their long life is mainly from the large value reached by $|Dst|$.

[3] The *Dst* (disturbance storm time) index is based on the H-component of the geomagnetic field averaged over four near-equatorial observatories. The strength of geomagnetic storms can be measured by the *Dst* index. In the case of an isolated magnetic storm, the *Dst* decreases drastically in the main phase and then recovers gradually to its quiet time level in the recovery phase. An isolated magnetic storm normally lasts for 1 day with a typical main phase of 3–12 hours and a recovery phase lasting ∼14 ± 4 hours [e.g., *Dasso et al.*, 2002; *Tsurutani and Gonzalez*, 1997]. However, there are some geomagnetic storms, which have more complex structure and show multiple-step decreases in *Dst* in the main phase and/or recovery phases. These geomagnetic storms often have longer duration and higher intensity. We refer to geomagnetic storms with total duration exceeding 3 days as long-lived geomagnetic storms (LLGMS).

[1]Catholic University of America, Washington, D.C., USA.
[2]Also at NASA Goddard Space Flight Center, Greenbelt, Maryland, USA.
[3]NASA Goddard Space Flight Center, Greenbelt, Maryland, USA.
[4]National Center for Radio Astronomy, Tata Institute of Fundamental Research, Ooty, India.
[5]Instituto de Geofisica, National Autonomous University of Mexico, Mexico City, Mexico.
[6]Atmospheric, Oceanic, and Space Sciences, University of Michigan, Ann Arbor, Michigan, USA.

0148-0227/06/2005JA011287

[4] It is now well established that coronal mass ejections (CMEs) are the major causes for large geomagnetic storms ($Dst < -100$ nT) [*Brueckner et al.*, 1998; *Cane et al.*, 2000; *Gopalswamy et al.*, 2000, 2005; *Wang et al.*, 2002; *Webb et al.*, 2000; *Zhang et al.*, 2003]. High-speed streams (HSS) in corotating interaction regions (CIRs) cause only moderate to weak storms (-100 nT $< Dst < -50$ nT). CMEs on the Sun are intrinsically magnetic entities with large fields; they also compress any IMF at their leading regions when they travel through the interplanetary (IP) medium and interact with other IP CMEs (ICMEs) and/or the ambient solar wind driving IP shocks. *Manoharan et al.* [2004] studied the influence of CME interaction on propagation of IP shocks and found that the CME interaction tends to slow the shock. Southward magnetic field (B_s) in shock sheaths and ICMEs or magnetic clouds (MCs) contribute to the generation of the geomagnetic storms. *Burlaga et al.* [2001] studied a set of fast ejecta observed at 1 AU from 5 February 1998 to 29 November 1999 and found all MC events and two complex ejecta resulting from the interaction of multiple CMEs produced geomagnetic storms. When HSS encounter and interact with CMEs, they can further compress B_z and enhance geoeffectiveness [e.g., *Burlaga et al.*, 1987; *Burlaga*, 1995; *Gopalswamy et al.*, 2005].

[5] Severe LLGMS events are often associated with complex interplanetary interaction regions [e.g., *Burlaga et al.*, 1987; *Cane and Richardson*, 1997; *Crooker et al.*, 1998; *Burlaga et al.*, 2002, 2003]. The common feature of the interaction regions is that they have relatively high and complex magnetic fields, which may consist of two or more B_s structures and cause a multistep *Dst* decrease. Such a storm is the so-called multistep storm [*Tsurutani and Gonzalez*, 1997; *Kamide et al.*, 1998; *Gonzalez et al.*, 2001]. In general, multistep storms result from consecutive impacts of southward B_s in different regions on the magnetosphere. *Kamide et al.* [1998] performed a statistical analysis of more than 1200 geomagnetic storms for the period from 1957 to 1991 and found that geomagnetic storms with two-step intensifications last longer and have larger storm size than the single-step storms. *Grande et al.* [1996] studied the 23 March 1991 two-step magnetic storm and found that the first event was dominated by Fe^{+9} while the second by Fe^{+16}. The possible explanation for this is that the first event was caused by the B_s in the shocked sheath region, while the second was caused by the intrinsic fields in the MC since high charge states are associated with ICMEs [*Fenimore*, 1980; *Henke et al.*, 1998; *Gloeckler et al.*, 1999; *Lepri et al.*, 2001]. *Gonzalez et al.* [2001] showed that for some events the main phase might develop in more than two consecutive steps; these storms exhibit a slowly developed long-duration main phase and relate to complex southward B_s structure.

[6] *Kamide et al.* [1998] argued that the two-step storm may result from the superposition of two successive modest storms. However, this assumption might be oversimplified. More studies indicate that the multistep storms could not be the result of simple superposition of individual ring current developments [e.g., *Chen et al.*, 2000; *Kozyra et al.*, 1998, 2002]. *Chen et al.* [2000] demonstrated that two intervals of enhanced convection are not inherently more effective at producing a strong ring current than one longer interval. *Kozyra et al.* [1998] showed that the inner magnetosphere retains little or no memory of previous injections since earlier injections are swept out of the dayside magnetopause as new population for the plasma sheet moves into the inner magnetosphere. The authors suggested that preconditioning occurs in a multistep storm through the cumulative effects of the successive storms on the plasma sheet population [*Kozyra et al.*, 1998, 2002]. Another possibility is that previous storms prime the inner magnetosphere through the substorm-associated accumulation of O^+ ions injected from the ionosphere during intense storms [*Hamilton et al.*, 1988; *Daglis*, 1997].

[7] In this paper, we conduct a statistical study of LLGMS, successive CMEs, and interaction regions of complex ejecta, IP shocks, and HSS to investigate their effects on the duration and intensity of these storms. We identified 37 LLGMS events with $Dst < -100$ nT during 1998–2002. We studied the storm duration, storm intensity, IP driver of the storm, and the cause of associated B_s structures. We found that when the driver of the LLGMS is associated with multiple CMEs (64.9% of the cases), the duration of LLGMS events is well correlated with the number of participating CMEs in an LLGMS and the intensity of LLGMS has a good correlation with the degree of interaction (the number of CMEs interacting with a HSS event or with themselves, see definition in section 3). Also, we investigated the role of cumultive preconditioning from consecutive storms in the multistep ring current intensifications in LLGMS events.

2. Methodology

[8] We used the *Dst* index data from the World Data Center in Kyoto (http://swdcwww.kugi.kyoto-u.ac.jp/dstdir/) to identify the geomagnetic storms. The associated CMEs observed by the Solar and Heliospheric Observatory (SOHO) mission's coronagraphs were obtained from the CME catalog (http://cdaw.gsfc.nasa.gov/CME_list) [*Yashiro et al.*, 2004]. The solar source regions of the CME were identified from the online Solar Geophysical Data (SGD) as the location of the associated GOES X-ray flares in order to see if CMEs were frontside and traveling toward Earth. When GOES X-ray flare information was not available, we used movies from the Extreme-ultraviolet Imaging Telescope (EIT) on board SOHO and Yohkoh mission's soft X-ray telescope to identify the location of the eruption. In order to identify the ICMEs, we use Fe charge state data from Advanced Composition Explorer/Solar Wind Ion Composition Spectrometer (ACE/SWICS), the solar wind plasma density, temperature, and flow speed from the Solar Wind Experiment (SWE) aboard the Wind spacecraft; and the magnitude $|B|$ and the B_z component of the interplanetary magnetic field from Wind Magnetic Field Investigation (MFI). Also, we used the IP shocks from Wind online shock list (http://pwg.gsfc.nasa.gov/wind/current_listIPS.htm), the MC list from *Lepping et al.* [2005], the MC-like (MCL) structures from Wind MFI online list (http://lepmfi.gsfc.nasa.gov/mfi/MCL1.html), and the CME trajectories obtained from empirical CME arrival (ECA) model [*Gopalswamy et al.*, 2000, 2001] to identify the arrival of successive CMEs at 1 AU.

[9] The ECA model is based on the empirical interplanetary acceleration of CME, which was found to be

$$\begin{aligned} a &= 2.193 - 0.0054u_0 (s < d_1) \\ a &= 0 (s > d_1) \end{aligned} \tag{1}$$

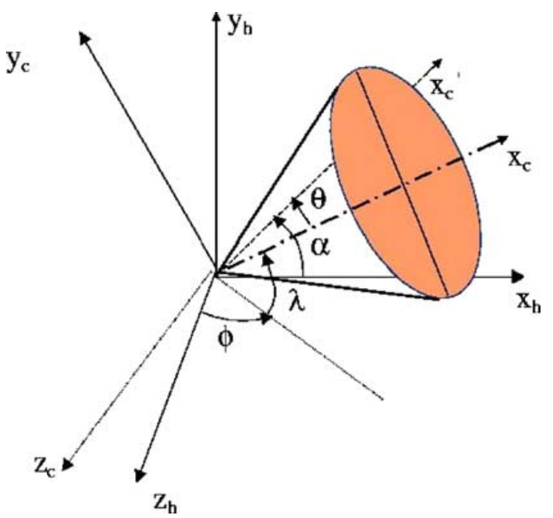

Figure 1. Topology of the cone model. The coordinate (x_h, y_h, z_h) is the heliocentric coordinate system, where z_h points to Earth, y_h points north, and the x_h - y_h plane defines the plane of the sky (POS). The coordinate (x_c, y_c, z_c) is the cone coordinate system, where x_c is the cone axis, and the y_c - z_c plane is parallel to the base of the right cone. The angles (ϕ, λ) are the longitude and latitude relative to the ecliptic plane. λ is the angle between the cone axis x_c and the x_h - y_h plane and ϕ is the angle between projection of x_c on the x_h - y_h plane and the z_h - axis. The angles (α, θ) are defined as the longitude and latitude relative to POS for conveniently determining the cone model parameters, where θ is the angle between x_c and POS and α is the angle between the cone axis projection on POS and x_h–axis.

where a is acceleration in units of m s^{-2}, and u_0 is initial CME speed in units of km s^{-1}, s is the heliocentric distance along the line of sight, d_1 is the acceleration ceasing distance. The ECA model assumed that the acceleration ceases at a distance d_1 in interplanetary space when the CME speed is the same as the ambient solar wind speed. Assuming d_2 = 1 AU − d_1, the CME travel time is computed as the sum of time t_1 to travel d_1 and t_2 to d_2: $t = t_1 + t_2$, where

$$t_1 = \frac{-u + \sqrt{u^2 + 2ad_1}}{a}, \ \mathrm{t}_2 = \frac{d_2}{\sqrt{u^2 + 2ad_1}}. \tag{2}$$

[10] The CME trajectories can be obtained from the basic kinematic equations:

$$\begin{aligned} s &= u_0 t + at^2/2(t < t_1) \\ s &= u_1 t + d_1(t > t_1) \end{aligned} \tag{3}$$

The ECA model requires the initial radial speed of a CME as input parameter. One of the difficulties in obtaining the CME initial speed is the uncertainty due to projection effects. Even though Earth-impacting CMEs typically originate from close to the Sun center [*Gopalswamy et al.*, 2000], there is no easy way to determine whether a halo or partial halo CME would reach Earth. In this work, we attempt to correct for the projection effect and resolve the criterion for a CME to reach Earth by an improved CME cone model [*Xie et al.*, 2004]. In the cone model, the orientation of a CME is defined by the longitude angle α (or φ) and the latitude angle θ (or λ); the angular width of the CME is defined by 2ω, as shown in Figure 1. The actual radial speed of the CME is given by

$$\mathrm{V_r} = \frac{dr}{dt} = \frac{V_{x_c\prime}}{\cos\omega\cos\theta - \sin\omega\sin\theta\sin\delta} \quad or \quad V_r = \frac{dr}{dt} = \frac{V_{y_c\prime}}{\sin\omega\cos\delta}, \tag{4}$$

where $V_{xc'}$ and $V_{yc'}$ are the components of the CME projection speed along $x_{c'}$ and $y_{c'}$ axes in the plane of the sky (POS), respectively, δ is the azimuthal angle defined as δ =

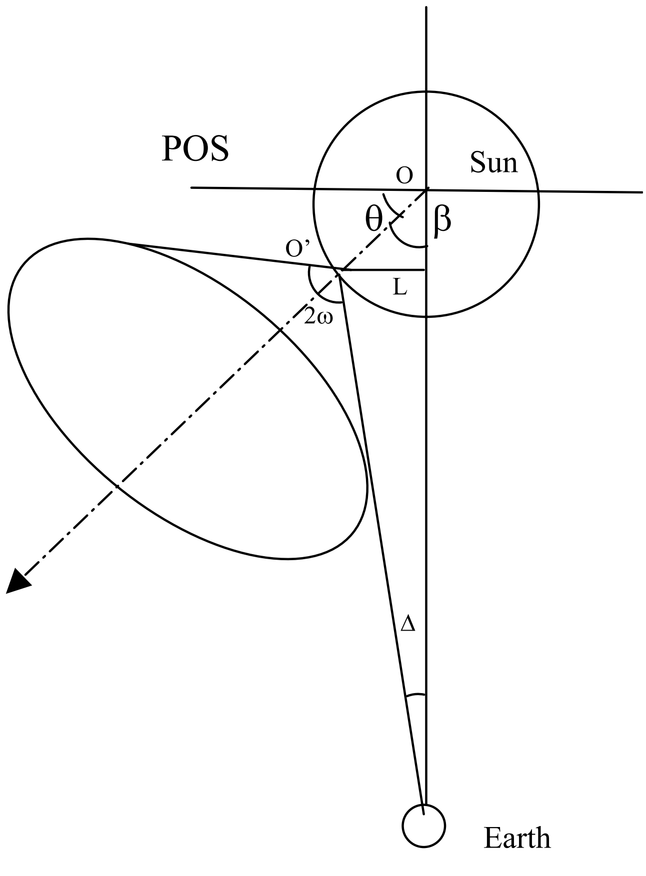

Figure 2. Illustration of the constraint ω ≥ β + Δ between the angular width 2ω and orientation (β, Δ) for a front-side halo (Δ = 0) or partial halo CME to encounter Earth. O is the solar disk center. O' is any arbitrary point on the solar surface near the disk center. Here β is the angle between the cone central axis and the line-of-sight (LOS). Here θ is the angle between the cone central axis and the plane of the sky. L is the distance of O′ to the LOS, and Δ is the angle between the LOS and one (Earth-directed) of the cone lateral projections.

Table 1. Successive CME Association With Long-Lived Geomagnetic Storms

Num	Dst_min Time,[a] UT	Dst_min,[b] nT	Start,[c] UT	End,[d] UT	Dur,[e] day	IP Driver[f]	CME[g]	Source Loc.[h]	Category and Comments[i]
						1998			
1	0218 0100	−100	0217 1200	0221 0100	~3.5	MC + HSS	0214 0655 (pH)	S24E23	S: (1, 1, h)
2	0307 0000	−116	0310 1100	0317 1000	~8.1	HSS in CIR	-	-	C: (0, 0, h)
3	0504 0600	−205	0502 0200	0508 0000	~5.9	Sh. + C. ICME	0429 1658 (H)	S18E20	M: (5, 3)
							0501 2340 (H)	S18W05	
							0502 0531 (H)	S20W07	
							0502 1406 (H)	S15W15	
							0503 2202 (pH)	S13W34	
4	0806 1200	−138	0806 0000	0809 1400	~3.6	MC + HSS	DG	-	S: (1, 1, h)
5	0827 1000	−155	0826 0900	0901 0900	~6.0	Sh. + MCL+ HSS	DG	-	S: (1, 1, h)
6	0925 1000	−207	0925 0100	0929 1300	~4.5	Sh. + MC + HSS	DG	-	S: (1, 1, h)
7	1019 1600	−112	1019 0000	10/23 1400	~4.6	MC + HSS	10/15 1004 (H)	N22W01	S: (1, 0, h)
8	1108 0700	−149	1108 2100	1112 0800	~3.5	C. ICME	11/05 0202 (H)	N19W10	M: (3, 2)
							11/05 2044 (H)	N22W18	
							11/06 0218 (pH)	N19W24	
9	1113 2200	−131	1113 0000	1117 1200	~4.5	Sh. + 2 MCL + HSS	11/09 1818 (pH)	N18W02	M: (2, 1, h)
							11/10 0618 (pH)	N17W08	
						1999			
10	0218 1800	−123	0218 400	0221 1400	~3.5	Sh. + C. ICME	DG	-	M: (3, 2)
11	1022 0700	−237	1021 0400	1029 1900	~8.6	MCL + HSS	10/19 0550 (pH)	S24E18	S: (1, 1, h)
12	1113 2300	−106	1110 2300	1115 2100	~4.9	HSS + C. ICME	DG	-	M: (2, 0, h)
						2000			
13	O212 1200	−133	0211 0400	0216 0100	~4.9	C. ICME + Sh. + HSS	02/08 0930 (H)	N25E26	M: (4, 3, h)
							02/09 1954 (H)	S17W40	
							02/10 0230 (H)	N31E04	
							02/12 0431 (H)	N26W26	
14	0407 0100	−288	0406 1800	0412 1200	~5.8	MCL + HSS	0404 1632 (H)	N16W66	S: (1, 2, h)
15	0524 900	−147	0523 2000	0526 2200	~3.1	C. Sh. + ICME	0522 0126 (H)	S20W48	M: (2, 2)
							0520 1450 (pH)	S21W30	
16	0716 0200	−301	0715 1600	0718 2000	~3.2	Sh. + MC	07/14 1054 (H)	N22W07	S: (1, 2)
17	0812 1000	−235	0810 300	0814 2200	~4.8	2 MCs	08/09 1630 (H)	N11W11	M: (3, 2)
							08/06 1830(pH)	N10E30	
							0810 0654 (pH)	N18E00	
18	0918 0000	−201	0917 2000	0921 2200	~4.1	Sh. + 3 MCLs	09/15 2150 (H)	N12E04	M: (4, 2)
							09/16 0518 (H)	N14W07	
							0915 1206 (pH)	N13E08	
							0915 1526 (pH)	N12E07	
19	1005 1400	−182	1002 0700	1008 1300	~6.3	Sh. + 4 MCLs	1002 0350 (H)	S09E07	M: (6, 3)
							1002 2026 (H)	S09E00	
							0929 2150 (pH)	S11E13	
							0930 1806 (pH)	S20E42	
							1001 1350 (pH)	S10E15	
							1003 0806 (pH)	N27W59	
20	1107 0200	−159	1105 1400	1108 1100	~3.1	Sh. + 3 ICMEs (2 MCLs)	1103 1826 (H)	N02W02	M: (3, 2)
							11/02 1626 (pH)	N23W58	
							1104 0150 (100)	S27 W30	
21	1129 1400	−119	1126 1600	1202 900	~5.4	Sh. + C. ICME	10 Halos	-	M: (10, 2)
						2001			
22	0331 0900	−387	0330 2300	0403 2100	~3.9	Sh. + MCL	03/28 0127 (H,)	N20E22	M: (4, 4)
							03/28 1250 (H)	N18E02	
							03/29 1026 (H)	N20W19	
							03/29 0026 (106)	N17W04	
23	1003 1500	−166	0925 2200	1005 1400	~9.7	Sh. + HSS + C. ICME	0924 1030 (H)	S16E23	M: (4, 2, h)
							0928 0854 (H)	N10E18	
							0929 1154 (H)	S13E03	
							0928 1030 (pH)	S18W36	
24	1021 2200	−187	1021 1800	1025 1000	~3.7	Sh. + C. ICME	1019 0127 (H)	N16W18	M: (3, 2)
							1019 1650 (H)	N15W29	
							1018 2026 (pH)	S17E69	
25	1028 1200	−157	1028 400	1031 1400	~3.4	Sh. + C. ICME	1025 1526 (H)	S16W21	M: (2, 0)
							1026 2050 (105)	N09E08	
26	1106 0700	−292	1105 1900	1112 1000	~6.6	Sh. + C. ICME +HSS	11/01 2230 (H)	N12W23	M: (3, 3, h)
							11/03 1920 (H)	N03W16	
							11/04 1635 (H)	N06W18	
27	1124 1700	−221	1124 0700	1128 0900	~4.1	Sh. + C. ICME (2 MCL)	1121 1406 (H)	S14W19	M: (3, 3)
							1122 2030 (H)	S25W67	
							1122 2330 (H)	S17W24	

Table 1. (continued)

Num	Dst_min Time,[a] UT	Dst_min,[b] nT	Start,[c] UT	End,[d] UT	Dur,[e] day	IP Driver[f]	CME[g]	Source Loc.[h]	Category and Comments[i]
						2002			
28	0420 0900	−149	0417 1200	0423 0500	~5.7	Sh. + MC +HSS + MCL	0415 0350 (H)	S15W01	M: (2, 1, h)
							0417 0826 (H)	S14W34	
29	0523 1800	−109	0522 0200	0526 0200	~4.0	C. Sh. + HSS	0522 0350 (H)	S30W34	M: (3, 0, h)
							0521 2150 (pH)	N17E38	
							0522 0006 (pH)	S20W70	
30	0821 0700	−106	0819 0000	0822 1900	~3.8	Sh. + C. ICME (2 MCs)	0816 1230 (H)	S14E20	M: (4, 0)
							0818 2154 (pH)	S08W28	
							0819 1106 (pH)	S12W19	
							0820 0154 (pH)	S11W35	
31	0904 0600	−109	0903 2000	0907 0000	~3.2	HSS in CIR	-	-	C: (0, 0, h)
32	0908 0100	−181	0907 0100	0915 1000	~10.4	Sh. + C. ICME + HSS	0905 1654 (H)	N09E28	M: (4, 2, h)
							0906 1331 (H)	N11W45	Pre. − 27 nT
							0904 1331 (pH)	S15E07	
							0908 1506 (pH)	N12E76	
33	1001 1700	−176	0930 200	1003 1000	~3.3	Sh. + MC	0928 0131(89)	N11E36	M: (3, 3)
							0928 1106(79)	N12E33	
							0929 0806 (106)	S08W70	
34	1004 0900	−146	1003 1000	1006 1500	~3.2	Sh. + 2 MCs	1002 0731 (pH)	S18E20	M: (3, 0)
							1003 0354 (pH)	S19E06	Pre. − 45 nT
							1003 0554 (pH)	N13W29	
35	1007 0800	−115	1006 1500	1013 1300	~6.9	HSS in CIR	-	-	C: (0, 0, h)
36	1014 1400	−100	1013 1300	1021 0600	~7.7	HSS in CIR	-	-	C: (0, 0, h)
37	1121 1100	−128	1121 300	1126 2200	~5.8	HSS in CIR	-	-	C: (0, 0, h)

[a]Dst minimum time of the LLGMS.
[b]Dst minimum value of the LLGMS.
[c]Start time of the LLGMS.
[d]End time of the LLGMS.
[e]Duration of the LLGMS.
[f]Interplanetary driver causing southward IMFs. MCL = Magnetic Cloud Like, Sh. = Sheath, C. = Compressed or Compound.
[g]Associated CME first appearance time in C2. Halo = Full Halo CME, pH = Partial Halo CME. If related CMEs are neither Halo or partial Halo, then their angular width are listed. DG = Data Gap.
[h]Solar source location of the associated CMEs.
[i]M = Multiple CME, S = Single CME, C = CIR. The first number in parentheses is the number of associated CMEs, second number is the degree of interaction: the degree of 1 represents interaction between a CME and a HSS, otherwise, the degree is equal to the number of CMEs involved in the possible interaction, h = cases involving HSS events.

$\tan^{-1}(z_c/y_c)$ in the cone coordinate. The projection speed $V_{r'}$ on POS along the position angle (*PA*) is related to $V_{xc'}$ and $V_{yc'}$ as follows: $V_{xc'} = V_{r'} \sin(\alpha - PA)$ and $V_{yc'} = V_{r'} \cos(\alpha - PA)$.

[11] The criterion for a CME to arrive at Earth is given by

$$\omega \geq \beta + \Delta, \tag{5}$$

where β is the angle between the cone central axis and the line-of-sight (LOS), L is the displacement of the CME source region to LOS, and Δ is the angle between the LOS and one (earthward) of the cone lateral projections, Δ = L/1 AU (see Figure 2) [*Xie et al.*, 2004].

3. Data

[12] Table 1 lists the 37 LLGMS events. In the table, the *Dst* minimum ($Dst_{\min}$) time, $Dst_{\min}$ value, storm onset time, storm end time, storm duration, IP driver, CME first appearance time in C2, associated solar source location, storm category, and comments are listed. The storm onset time is defined by the occurrence time of storm sudden commencement (SSC), which is caused by an intensification of the magnetopause current as the enhanced solar wind dynamic pressure (due to the IP shock) drives the magnetopause inward. The SSC is normally associated with the occurrence of IP shocks but may not be recognizable when the geomagnetic field is already depressed (preconditioning). When there is no clear identification of an SSC, we define the storm onset time as the time when *Dst* starts decreasing. The storm end time is defined by the time when the *Dst* recovers to $Dst_0(1/e)$, where Dst_0 is −50 nT, the minimum intensity of modest storms. The LLGMS events are classified as (1) multiple CME (M) type, (2) single CME (S) type, and (3) CIR (C) type. In column 10, the first number in parentheses represents the number of participating CMEs in an LLGMS. The criterion to determine the number of participating CMEs in the LLGMS is to examine whether the arrival time of CMEs from the ECA model falls into the interval of LLGMS plus an error of ±21.4 hours, i.e., two times of root-mean-square (rms) of ECA model, where the average prediction error (rms) was estimated as 10.7 hours [*Gopalswamy et al.*, 2001]. The second number in column 10 represents the degree of interaction, which is defined as follows: if the interaction occurs between a CME and a HSS, the interaction is of degree 1; otherwise, the degree is equal to the number of CMEs involved in the possible interaction. We applied criterion (5) to identify if a CME has a component heading toward Earth [*Xie et al.*, 2004] and extrapolated the CME trajectories from the Sun to 1 AU (see bottom panel of Figures 3a and 3b). If the trajectories of two CMEs intersect, then it indicates that an

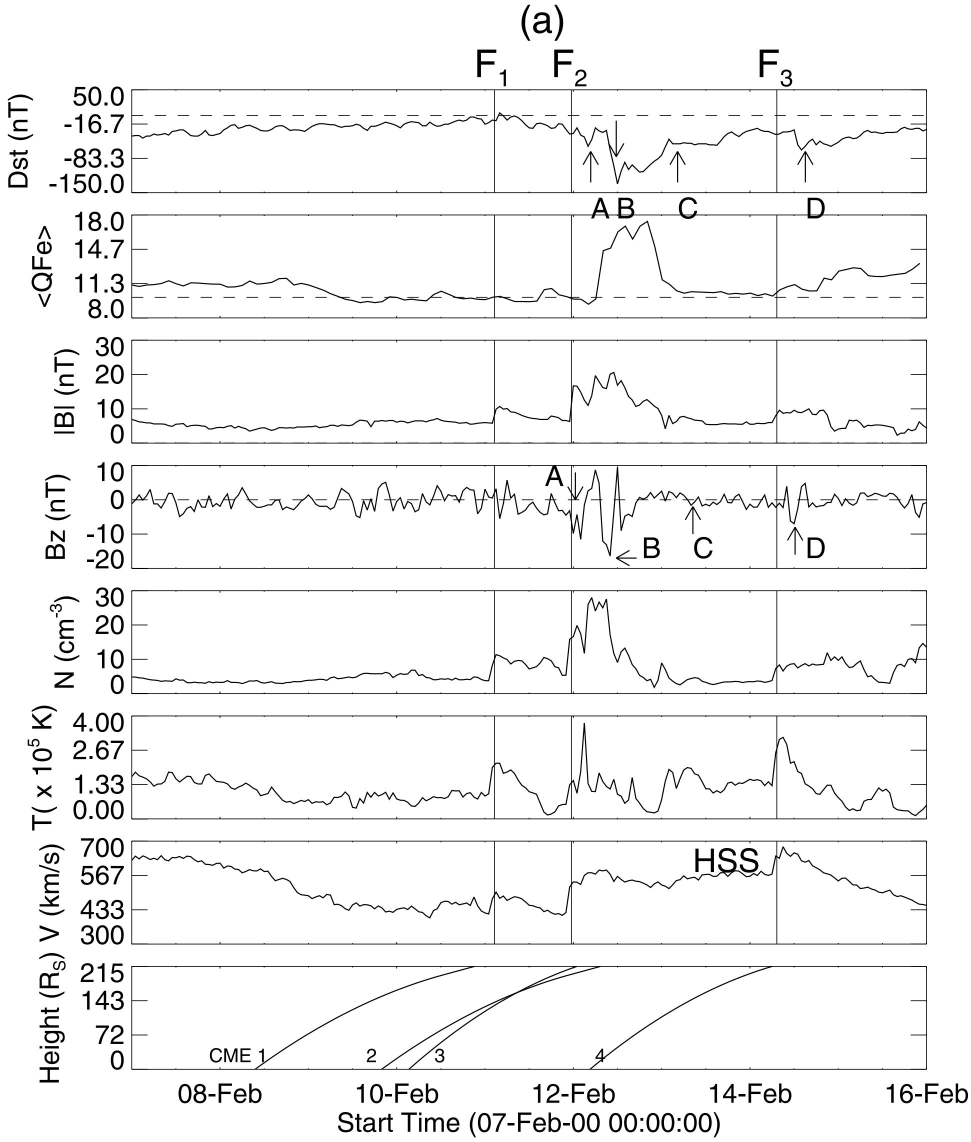

Figure 3a. A LLGMS associated with successive CMEs. From top to bottom: the panels are D_{st} Index, Fe charge state, $|B|$, B_z, N, T, V and CME height-time profile, respectively. The vertical solid lines indicate the ICME shock front (F_1, $_2$, $_3$, $_4$, F denotes forward fast shock). The number on the bottom panel indicates the associated CMEs. The arrows show the dips in complex structures of D_{st} and B_z. Note that the drop in $\langle Q_{Fe} \rangle$ near F_2 is due to the instrumental noise produced by the impact of the shock.

interaction has occurred between the two CMEs (the distance where the CME interaction occurs is indicated in the y-axis of the CME height-time plot). The third letter "h" in parentheses of column 10 denotes cases involving an HSS event.

[13] Figures 3a, 3b, 5, and 6 present four examples of LLGMS events, in which we show the associated *Dst* variation and related solar wind parameters. Figure 3a shows the *Dst* index, Fe charge state data $\langle Q_{Fe} \rangle$, $|\boldsymbol{B}|$ and B_z, solar wind density N, temperature T, flow velocity V, and the trajectories (height-time profiles) of the associated CMEs for the 12 February 2000 event. In this event the LLGMS lasted for $\sim$4.9 days (11–16 February). There were two dips (dip "A" and dip "B") in the main phase and two dips (dip "C" and dip "D") in the recovery phase (see arrows in the *Dst* plot). Four CMEs (labeled with numbers on the CME trajectories of Figure 3a) have been found to be associated with this event. Three forward fast shocks F_1 (on 11 February at 0233 UT related to CME 1), F_2 (on 11 February at 2338 UT resulting from the possible interaction of CME 2 and CME 3), and F_3 (on 14 February at 0718 UT corresponding to CME 4), were present in this event. CME 2 and CME 3 arrived at about the same time at $\sim$1 AU. It is likely that CME 3 has caught up with CME 2 and the two CMEs merged, resulting in a single complex ejecta (ICME 2). A MC (12 February, 1706 to 13 February, 0036) with a complex leading sheath region formed part of ICME 2. An anomalous high Fe charge state interval in the event corresponds to this complex ICME 2. Figure 3a shows that the ICME 2 has run into the rear part of ICME 1, causing compressed B_s in the trailing region of ICME 1. Possible interaction occurred between CME 1, CME 2, and CME 3.

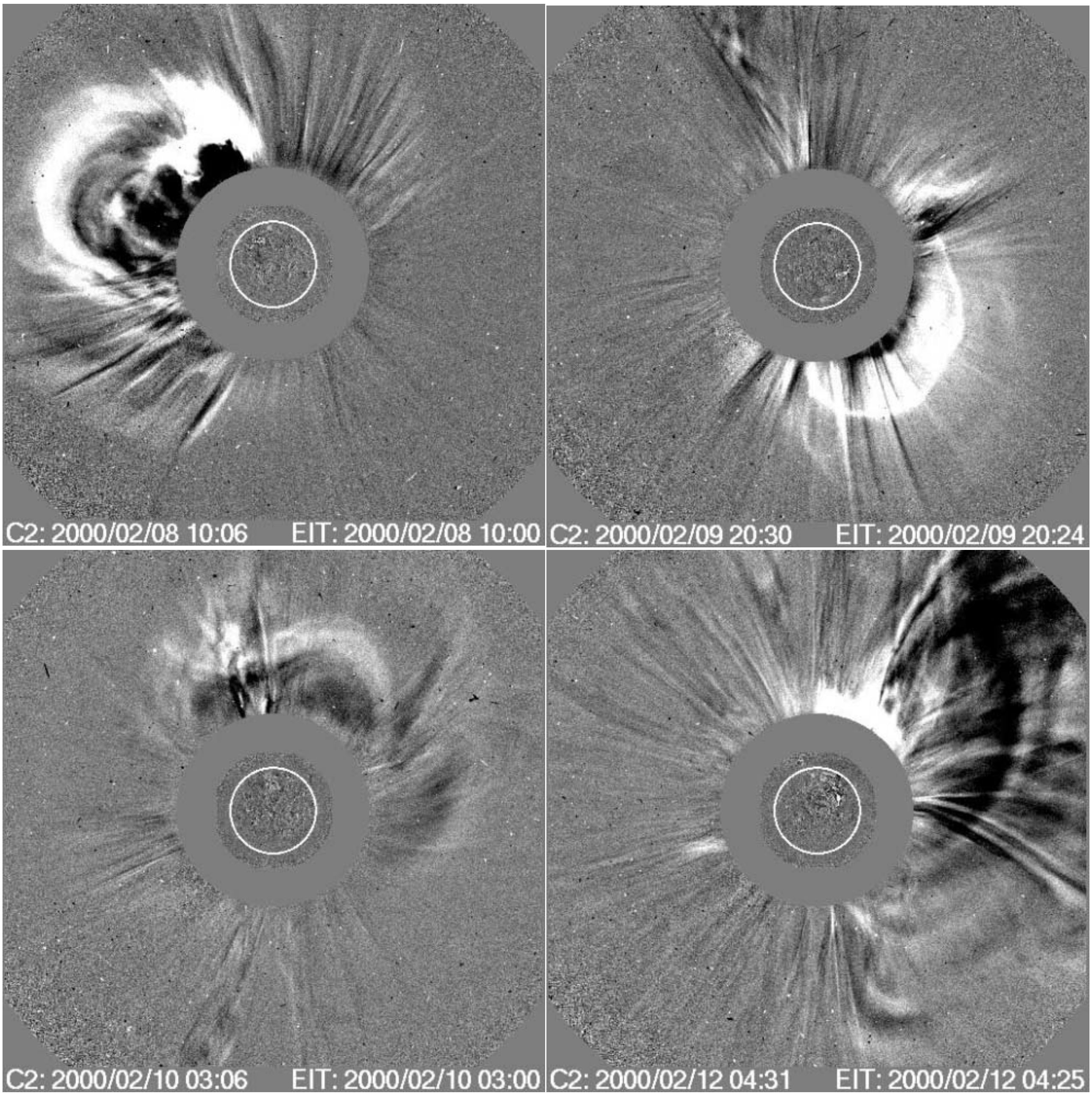

Figure 3b. LASCO C2 images of CMEs associated with the event. From top left to bottom right: CME 1, CME2, CME3, and CME 4.

Dip "A" in the main phase was caused by the compressed B_s in the rear part of ICME 1. Dip "B" followed by a small dip was produced by the B_s structures in the sheath region and the MC, respectively. The MC was followed by a HSS-like structure with high T and low N, causing Dip "C" in the recovery phase, where the *Dst* value was nearly constant for more than 10 hours. However, this HSS-like structure could also likely be the extension of the ICME 2, since no apparent coronal hole was observed at low latitude near the Sun disk (ICME interval is typically featured with low T and reduced field fluctations, but such features may not be present in some ICMEs [*Cane and Richardon*, 2003]). CME 1, CME 3, and CME 4 originated from the active region AR8858 when it was at N25E26, N31E04, and N26W26 as the Sun rotated westward. CME 2 originated from AR8853 at S17W40. Figure 3b shows the LASCO images of the four successive CMEs associated with this event, superposed with EIT images.

[14] Figures 4a and 4b shows the *Dst* index, $\langle Q_{Fe} \rangle$, $|\boldsymbol{B}|$, B_z, N, T, V, the trajectories of the associated CMEs and CME C2 images for the 20 April 2002 event. In this event the LLGMS extended from 17 April to 23 April and the storm lasted for $\sim$5.7 days. The LLGMS consists of two consecutive storms, which are associated with two successive MCs: MC 1 (18 April, 0418 to 19 April, 0218) and MC 2 (20 April, 1148 to 21 April, 1648). Two forward shocks F_1 (17 April at 1101 UT), F_2 (19 April at 2222 UT), and one reverse shock R_2 (20 April at 0440 UT) were found ahead of

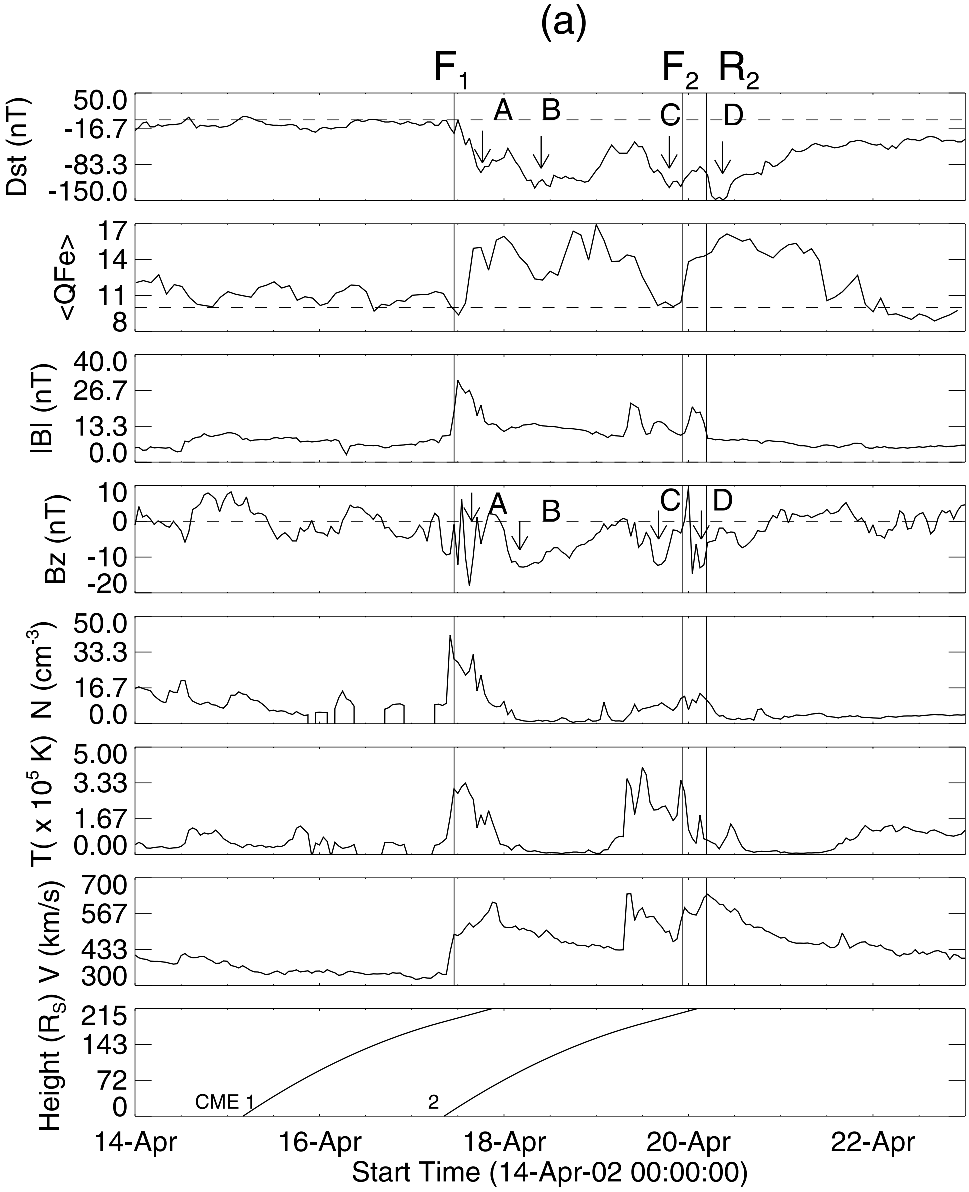

Figure 4a. A LLGMS associated with two IMCs. From top to bottom the panels are D_{st} index, Fe charge state, $|B|$, B_z, N, T, V and CME height-time profile, respectively. The vertical solid lines indicate the ICME shock front (F_1, F_2, R_2, F denote forward fast shock and R denotes reverse shock). The number on the bottom panel indicates the associated CMEs. The arrows show the dips in complex structures of D_{st} and B_z. Note that the drop in $\langle Q_{Fe} \rangle$ near F_1 due to the instrumental noise produced by the impact of the shocks.

the MC 1 and MC 2, respectively. The MC 1 produced a typical two-step ring current intensification, i.e., dip "A" and dip "B" in the *Dst* plot of Figure 4a, caused by the B_s in the sheath region and the cloud, respectively. This two-step feature was not seen in the second storm; only dip "D" was produced by the B_s in the sheath region of shock F_2. The solar origin of dip "C" was difficult to define since we did not find any reported CME on the Sun. It might be either due to a short HSS-like structure or an ejecta associated with a missing CME. Two CMEs, which caused the two MCs, respectively, were observed to be associated with this event. CME 1 originated from active region AR9905 at S15W01 with an M1.2 flare and CME 2 originated from active region AR 9906 at S14W34 with an M2.6 flare. Fe charge state data showed two clear anomalous stages for this event, and their onsets are in near coincidence with the leading edge of the MCs. Figure 4b shows LASCO C2 images of CME 1 and CME 2.

[15] Figure 5 shows the *Dst* index, $\langle Q_{Fe} \rangle$, $|\boldsymbol{B}|$, B_z, N, T, V, and the trajectory of the associated CME for the 7 April 2000 event. The LLGMS lasted 5.8 days, extending from 6 April 2000 to 12 April 2000 [*Gopalswamy*, 2002]. A fast forward shock F_1 on 6 April at 1627 UT and a reverse shock R_1 on 7 April at 0916 UT were present in this event. The *Dst* minimum of the LLGMS is $\sim$−288 nT, which was caused by the B_s in the sheath region of F_1. A HSS-like structure

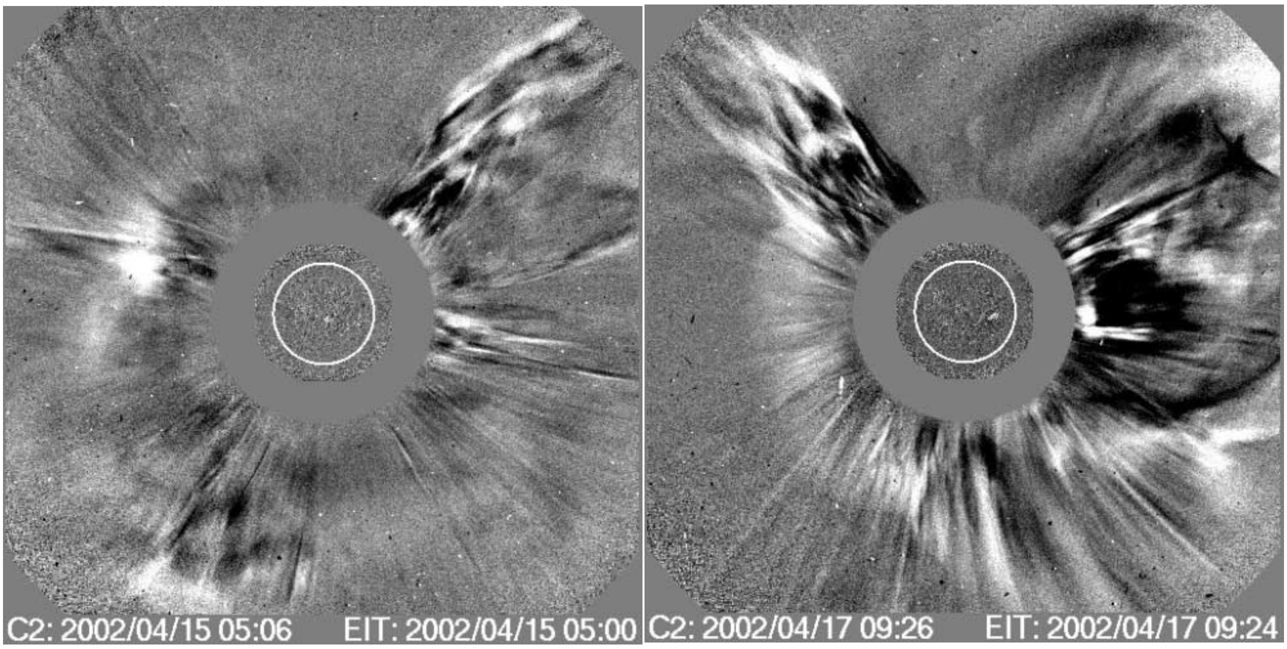

Figure 4b. LASCO C2 images of CME 1 and CME 2 associated with the event.

has caused the long recovery phase of the LLGMS. Shock F_1 was associated with a fast halo CME with actual speed of 1139 km/s and actual angular width of 128° obtained by the cone model.

[16] Figure 6 shows the corresponding data for the LLGMS from 6 October 2002 to 13 October 2002. The LLGMS had lasted for ~6.9 days with modest intensity of the minimum $Dst \sim -115$ nT. It was produced by a HSS emanating from a low-latitude coronal hole, which was present a few days earlier near the disk center at 2200 UT on the 5 October 2002 EIT image.

4. Statistical Results

4.1. Associations

[17] First of all we find that the LLGMS events were produced by complex B_s structures in various interaction regions: (1) IP shocks and complex ICMEs related to successive CMEs; (2) single IP shock and ICME (MC); (3) HSS events in CIRs. Note that both type 1 and type 2 might be mixing with possible HSS events. Of the 37 LLGMS events, 24 (64.9%) were associated with multiple CMEs, 8 (21.6%) were caused by single CMEs, and 5 (13.5%) were related to CIRs with no CME involvement.

4.2. LLGMS Properties

4.2.1. LLGMS Duration

[18] In order to study the relationship between the duration of LLGMS and successive CMEs and their interaction with HSS events, the LLGMS events were divided into the following six groups: (1) all multiple CME cases; (2) all single CME cases; (3) all CIR cases with no related CME; (4) multiple CME cases with >3 CMEs; (5) all cases involving HSS; (6) cases with no HSS and $\leq$ 2 CMEs. Note that the classification of the groups (1–6) does not imply disjunct sets, e.g., in this case group 4 is a subset of group 1. We use group 4 to study the effects of multiple CMEs (>3) on the duration (*Dur*) of LLGMS, and group 5 to study the effects of HSS events on *Dur*. Group 6 is used to study the cases without either multiple CMEs or HSS. Figure 7 presents the distribution of the duration of LLGMS for six different groups. The median durations for the above six groups are 4.1, 4.6, 6.9, 5.4, 5.8, and 3.4 days, respectively. In the multiple CME group, the LLGMS events were associated with more than one B_s structure and the *Dst* developed in multiple consecutive steps, causing the long duration. The median durations for the multiple CME type 1 and 4 are 4.1 and 5.4 days, respectively. The median duration for the CIR group is the longest with a median value of 6.9 days. The second-longest duration is for all the LLGMS events involving HSS. The nature of the duration in the events involving HSS is due to the long periods of B_s fluctuations within HSS. As expected, the median duration for group 6 with no HSS and $\leq$2 CME is the shortest among the six groups, with a median value of 3.5 days. Therefore the CIRs and HSS are associated with the largest duration LLGMS events. If an LLGMS is associated with successive CMEs, the duration of the storm increases with the number of the participating CMEs. Figure 9a shows the relationship between the LLGMS duration and the number (*nc*) of participating CMEs. We find that there is a good correlation between the duration and *nc* with correlation coefficient (*r*) of 0.78.

[19] Note that some single CMEs (with no HSS) events can reach long durations (~3 days) because of the very large storm intensity in these events, which caused relatively long recovery phase of the storms.

4.2.2. LLGMS Intensity

[20] To study the effect of the interaction CMEs with other CMEs and HSS on the intensity of LLGMS, we group the LLGMS events as in subsection 4.2.1, except that group 6 is classified as cases with no CME interaction. We extrapolated the CME trajectories from the Sun to 1 AU (see bottom panel in Figure 3a) to decide if two CMEs

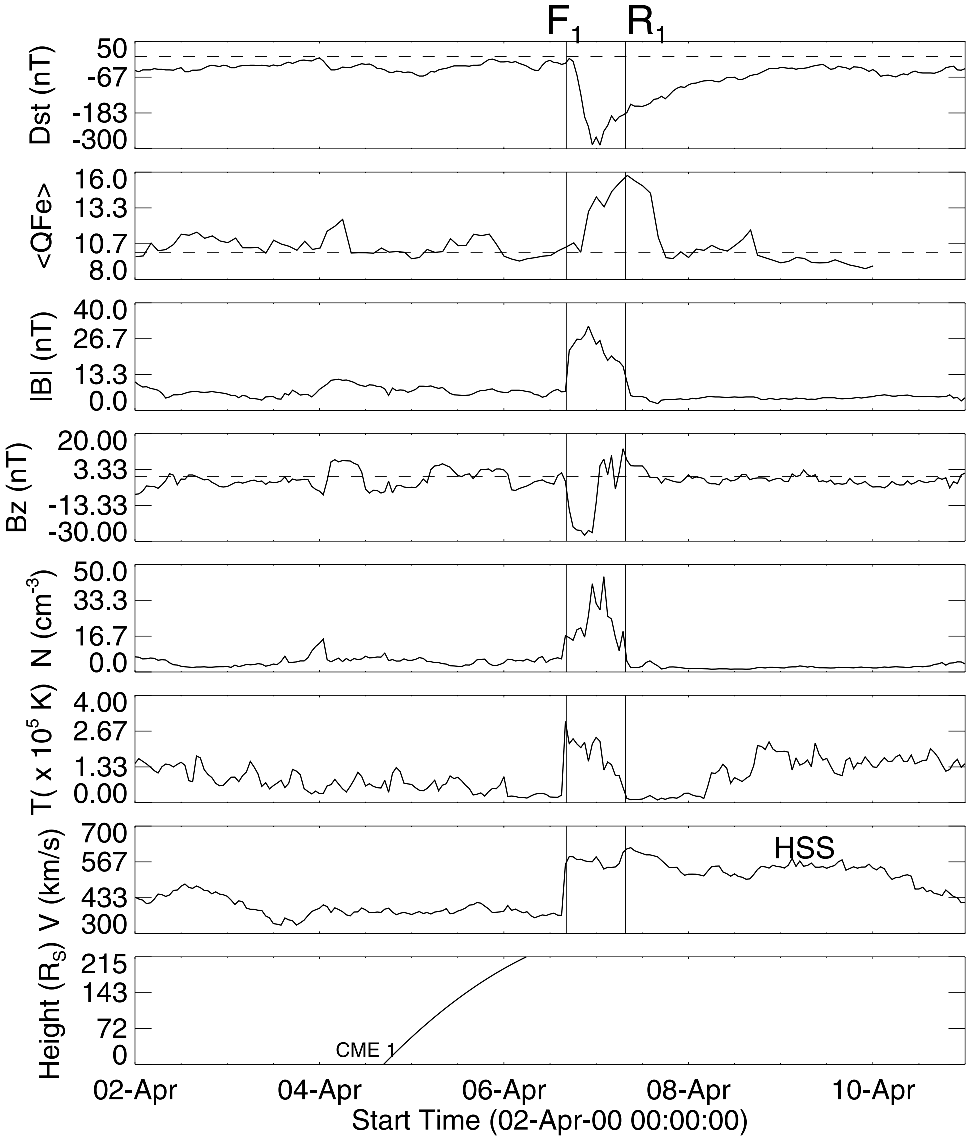

Figure 5. A LLGMS associated with a single CME event: corresponding solar wind data, IMF, and the D_{st} index from 2 April 2000 to 11 April 2000. The associated CME is a fast halo with an actual speed of 1139 km/s.

interact and applied criterion 5 to identify if a CME would reach Earth [*Xie et al.*, 2004]. Figure 8 presents the histogram of the $Dst_{\min}$ of LLGMS of the above groups. The median values of $Dst_{\min}$ for the six groups are -157, -155, -115, -181, -133, and -116 nT, repectively. The multiple CME groups possessed relatively large median $Dst_{\min}$ values with a median value of -157 nT for group 1 (all multiple CME cases) and -181 nT for group 4 (multiple CME with >3 CMEs). Group 3 (CIR cases) and group 5 (cases with HSS involved) exhibited modest median intensity with a median $Dst_{\min}$ of -115 nT and -133 nT, respectively. In the multiple CME group 4, the CME interaction may play an important role in enhancing the intensity of the LLGMS events. Figure 9a shows the relationship between the LLGMS intensity and the degree of interaction (*ni*) (see definition in section 3). It is found that the correlation coefficient (*r*) between the intensity and *ni* is 0.67.

4.3. Preconditioning in LLGMS Events

[21] The relationship of the intensity of magnetic storms to solar wind parameters can be examined using the Burton equation [*Burton et al.*, 1975]. Burton's equation has been tested and improved by numerous authors [e.g., *Clua de Gonzalez and Gonzalez*, 1998; *Fenrich and Luhmann*, 1998; *O'Brien and McPherron*, 2000; *Wang et al.*, 2003]. It is given by O'Brien and McPherron in a slightly different form:

$$\frac{dDst^*}{dt} = Q(t) - \frac{Dst^*(t)}{\tau}, \tag{6}$$

where the energy injection term

$$Q = \begin{cases} a(\mathrm{V}B_s - E_c) & VB_s > E_c \\ 0 & \mathrm{V}B_s < E_c \end{cases},$$

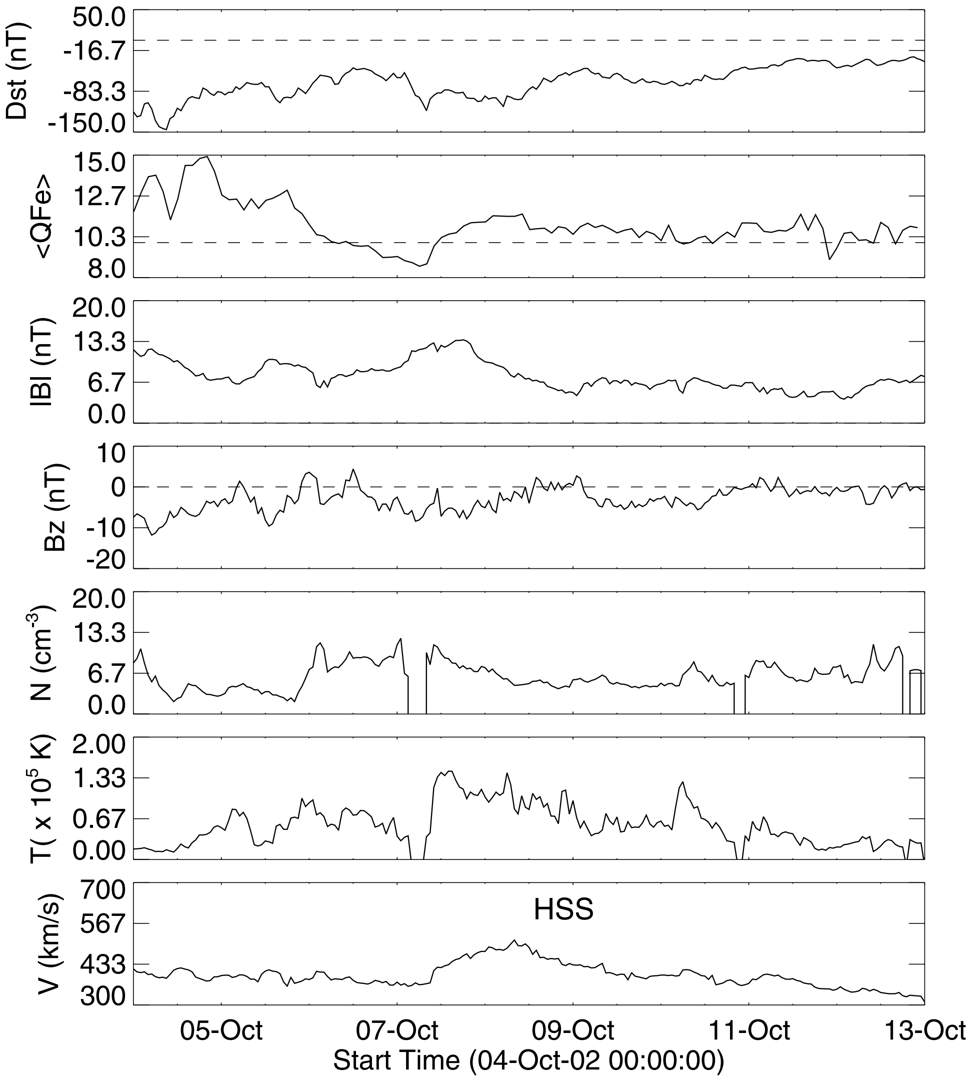

Figure 6. A LLGMS associated with a HSS event: corresponding solar wind data, IMF, and the D_{st} index from 4 October 2002 to 13 October 2002. There was a coronal hole a few days earlier near the disk center at 2200 UT in the 5 October 2002 EIT image (not shown).

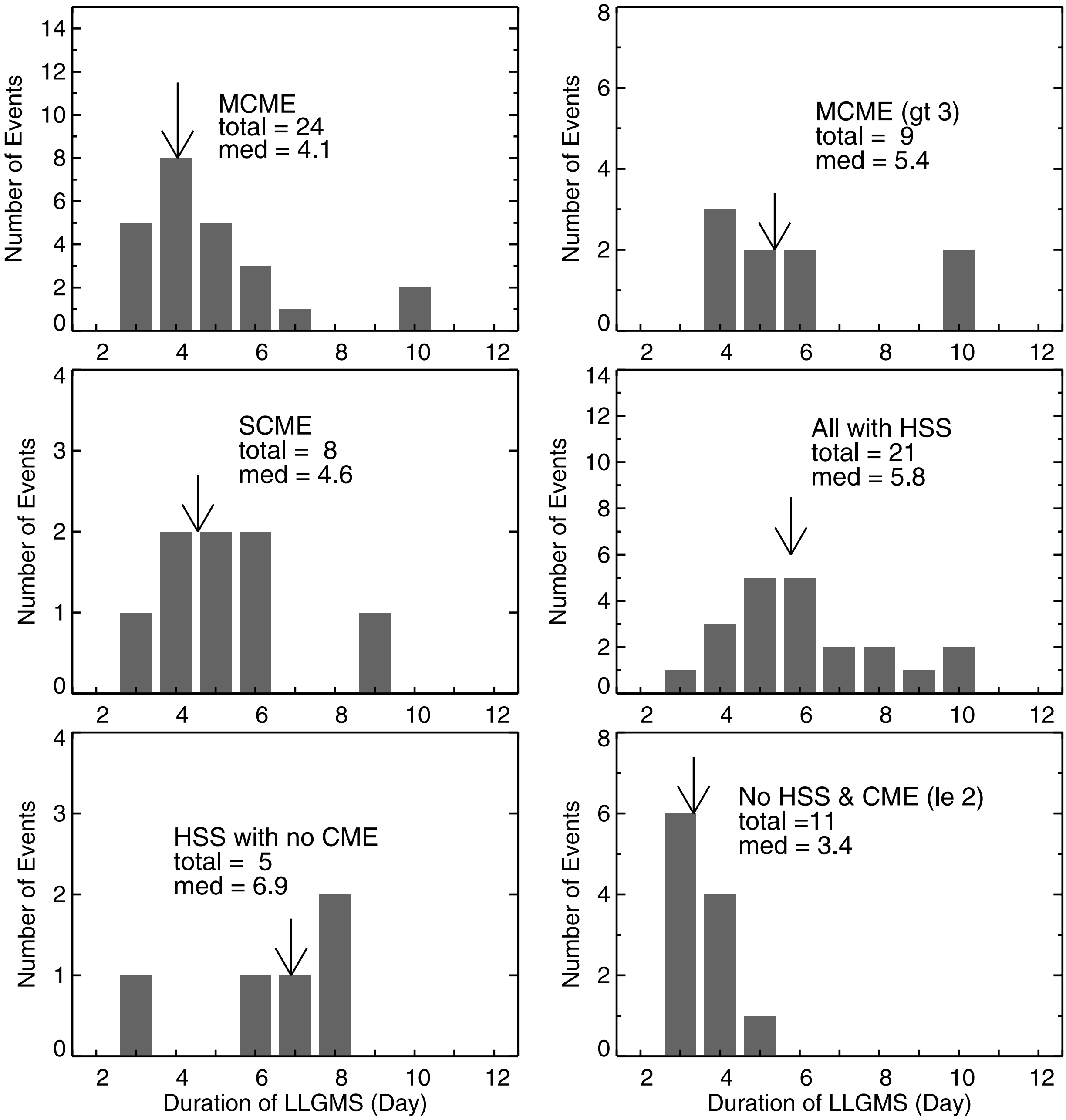

Figure 7. Histograms of durations for the six groups of LLGMS events. These six groups are (a) all multiple CME cases; (b) all single CME cases; (c) all CIR cases with no related CME; (d) multiple CME cases with >3 CMEs; (e) all cases with HSS involved; (f) cases with no HSS and $\leq$ 2 CMEs.

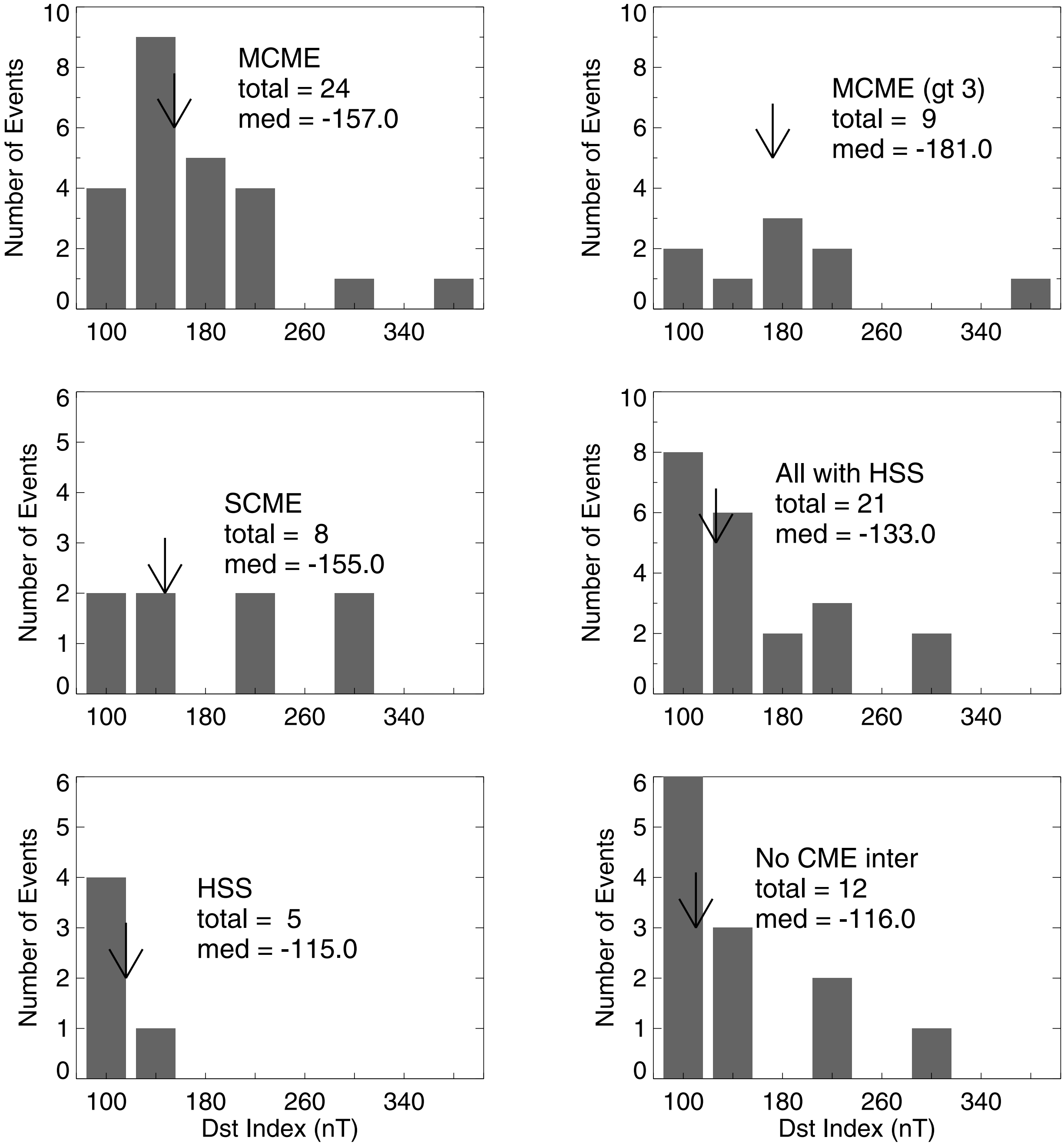

Figure 8. Histograms of *Dst* minimums (absolute value) for the six groups of LLGMS events. These six groups are (a) all multiple CME cases; (b) all single CME cases; (c) all CIR cases with no related CME; (d) Multiple CME cases with > 3 CMEs; (e) all cases with HSS involved; (f) cases with no CME interaction.

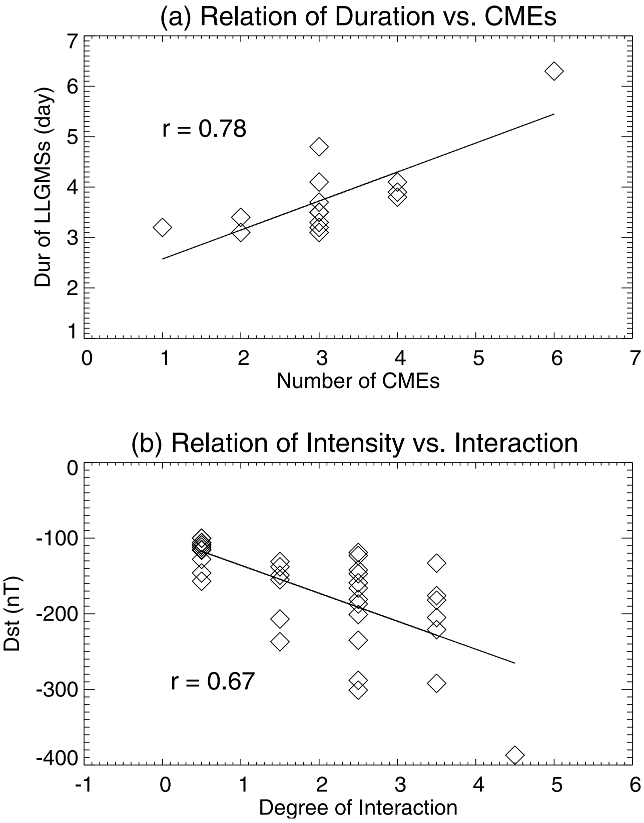

Figure 9. Relationships and correlation coefficients for (a) LLGMS duration and the number of associated CMEs (*nc*); (b) LLGMS intensity and the degree of interaction (*ni*).

V is the solar wind flow speed, VB_s is the solar wind dawn-dusk electric field, the proportional constant a is -4.4 nT/h(mV/m)$^{-1}$ and the electric field threshold E_c is 0.49 mV/m. The pressure-corrected index $Dst^* = Dst - b\sqrt{p} + c$, from which the contribution of the magnetopause current to Dst has been removed, p is the solar wind dynamic pressure, b is a constant of proportionality, and c is a constant representing the changes of both the quiet time magnetopause and the ring currents, and τ is the decay time of the ring current, associated with loss processes in the inner magnetosphere. O'Brien and McPherron's improved model has also considered the influence of VB_s on τ as follows: $\tau = 2.40 \exp[(9.74/4.69 + VB_s)]$ with VB_s in mV/m. More recently, *Wang et al.* [2003] suggested that the O'Brien and McPherron's model can be further improved by $Q = a(VB_s - E_c)(p/p_0)^\gamma$, where the index γ and the constant p_0 are optimized by minimizing the root-mean-square (RMS) errors.

[22] The empirical *Dst* model combined with the statistically derived decay time have had remarkable success in predicting the strength of geomagnetic storms (see review by *Gonzalez et al.* [1994]). However, Burton's formula and its variations [e.g., *O'Brien and McPherron*, 2000; *Wang et al.*, 2003] depend only on the solar wind coupling value VB_s and does not take into account any preexisting condition in the magnetosphere, so they might not be applicable for the multistep *Dst* development of LLGMS events when preconditioning occurs due to the presence of successive storms. In order to investigate whether Burton's formula and its variations are applicable for the *Dst* development of LLGMS, we studied the relationship between B_s, VB_s, and $Dst_{\min}$. We divided the LLGMS events as individual ring current intensifications, i.e., individual *Dst* dips in the main and recovery phases. We identify the *Dst* dips according to the following conditions: (1) $Dst_{\min}$ must be less than -50 nT; (2) two consecutive dips must be separated by more than 3 hours; (3) the magnitude of the decrease of $Dst_{\min}$ in a dip must be less than -30 nT or $Dst_{\min}$ remains the same level (see Figure 3a as an example) for more than 6 hours. We use the first criterion to exclude weak storms, which are mostly caused by HSS events. The second criterion excludes cases in which apparent decreases in *Dst* were caused by substorm effects such as the so-called current wedge, not a true increase in the storm time ring current [*Kamide et al.*, 1998]. The third criterion is employed to help distinguish a well-defined dip.

[23] Figure 10 shows the relationship between $Dst_{\min}$, B_s, and VB_s. From top to bottom, this figure shows the results for: all *Dst* dips, *Dst* dips in the main phase, and *Dst* dips in the recovery phase, respectively. As expected, in general, $Dst_{\min}$ is well correlated with B_s ($r = 0.79$) and VB_s ($r = 0.80$). In the main phase, $Dst_{\min}$ has a better correlation with both B_s ($r = 0.79$) and VB_s ($r = 0.84$). In the recovery phase, however, the correlation relation between $Dst_{\min}$, B_s, and VB_s is relatively poor, with coefficients of 0.59 and 0.60, respectively. The results imply that in the main phase the preconditioning of previous storms may not play a significant role in the multiple development of *Dst* since each *Dst* dip acts as a separately existing storm in this stage. However, in the recovery phase the effect of preconditioning on the *Dst* development cannot be ignored. This is due to the fact that in the recovery phase the *Dst* recovery and *Dst* decay (of later consecutive storms after *Dst* negative peak) occurs at the same time in the LLGMS events. After the maximum intensification of the ring current, the cumulative effects of prior storms on plasma sheet characteristics will change the response of the magnetosphere to solar wind drivers, as proposed by *Kozyra et al.* [1998, 2002].

5. Summary and Discussion

[24] We investigated 37 LLGMS events from 1998 to 2002. We find three causes of LLGMS events: (1) multiple CMEs (64.9%, 24 of 37); (2) single CME (21.6%, 7 of 37); (3) HSS in CIRs (13.5%, 5 of 37). The first two causes of LLGMS events involved possible HSS events, causing complex interaction regions in the interplanetary medium. In the multiple CME cases, the associated IP driver is a merged interaction region involving IP shock, complex ejecta, and HSS. The LLGMS events involving multiple CME have medium long duration and high intensity due to successive CMEs and various interactions. The single CME cases generally involve a fast halo CME associated with a very strong interplanetary shock, which produces super intensity (>-280 nT) storm. In the CIR cases, the LLGMS events have modest intensity ($\sim$100 nT) but the longest duration due to extended periods of the highly fluctuating B_s within HSS.

[25] If an LLGMS is associated with interacting CMEs, there is a good correlation between the number of CMEs involved in an LLGMS and the LLGMS duration with

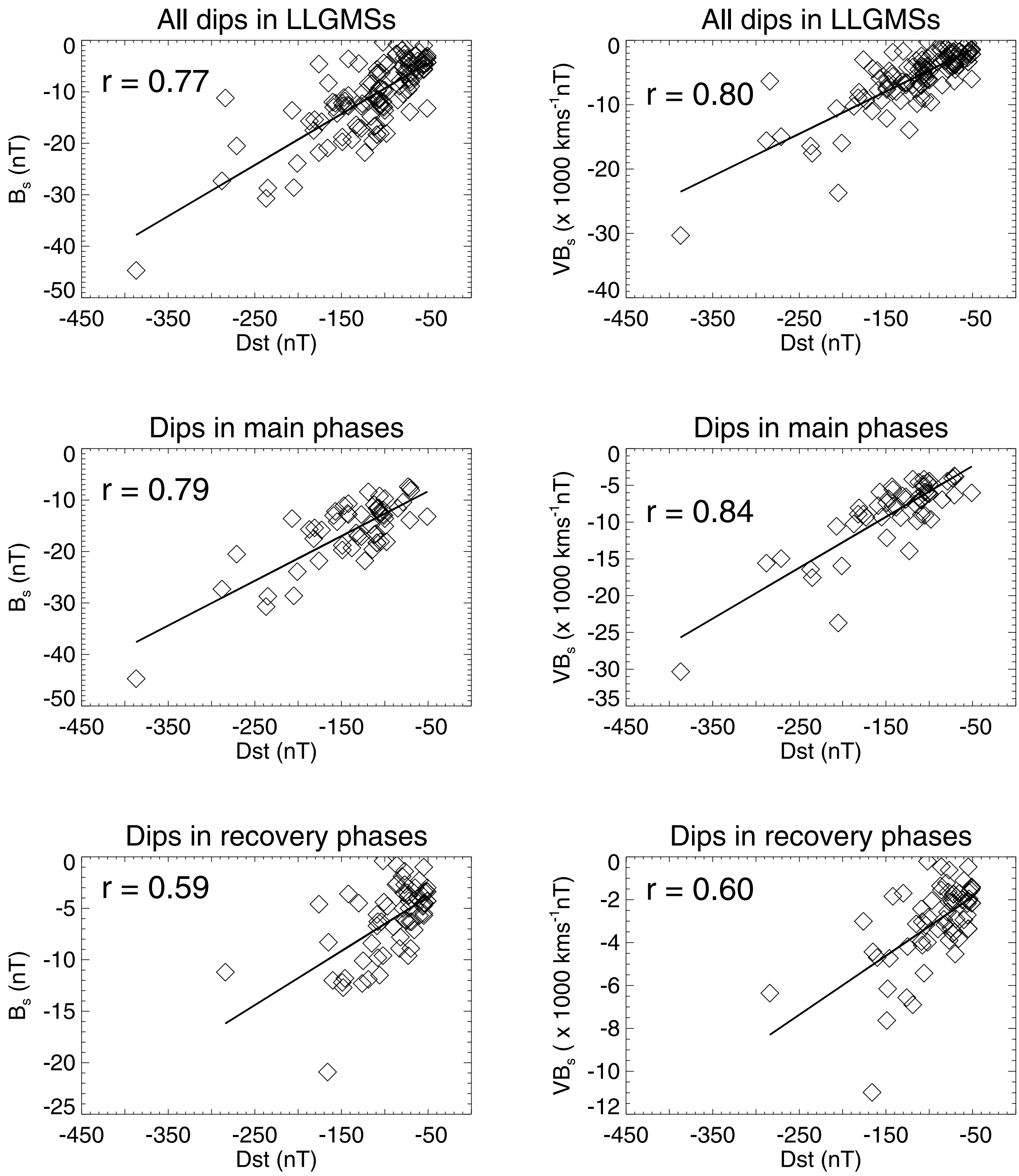

Figure 10. Relationships of $Dst_{\min}$ with B_s and VB_s. From top to bottom, panels are the results for all dips in LLGME events, dips in main phases, and dips in recovery phases, respectively.

correlation coefficient $r = 0.78$. Interaction between successive CMEs plays an important role in enhancing the intensity of the LLGMS events. The intensity of LLGMS is well correlated with the degree of interaction (i.e., the number of CMEs interacting with HSS or with themselves in the associated interaction region) with $r = 0.67$. Of the 37 LLGMS events we studied, there were 20 (54.1%) events involving possible CME interaction. The largest LLGMS during 1998–2002 is the 31 March 2001 event with $Dst_{\min} \sim -387$ nT, which was involved four successive CMEs interacting with one another. Note that there are cases of interacting CMEs which do not trigger LLGMS due to unfavorable northward IMF conditions. Our analysis does not include these cases because we are interested in the solar origin of the existing LLGMS.

[26] As we expected, there is a good correlation between $Dst_{\min}$, B_s, and VB_s. The correlation of $Dst_{\min}$ with B_s for all the dips in LLGMS events is 0.77 and for the dips in the main phases it is 0.79. The correlation of $Dst_{\min}$ with VB_s is slightly better than with B_s with $r = 0.80$ and 0.84, respectively, for all dips and main phase dips. However, in the recovery phases, the correlation relation is relatively poor, with coefficients of 0.59 and 0.60 between $Dst_{\min}$ and B_s, VB_s, respectively.

[27] Our results suggest that the preconditioning may have little effect on multiple *Dst* development in the main phase of LLGMS, while it does affect the recovery phase. The reason is that the recovery phase involves both the ring current decay of prior storms and intensification of later storms in an LLGMS event. After the *Dst* negative peak, the cumulative effects of prior storms on plasma sheet characteristics will alter the response of the magnetosphere to subsequent solar wind drivers, as suggested by *Kozyra et al.* [1998, 2002]. However, how the plasma sheet responds to the solar wind driver and how it is affected by the preexisting storms are still not well understood. Further detailed investigation on the preconditioning is needed.

[28] **Acknowledgments.** The authors would like to thank the support of ACE/SWICS, ACE/SWEPAM, WIND/MFI teams, and NSSDC center for processing data. This work was supported by NASA LWS and NSF SHINE (ATM 0204558) program. AL thanks UNAM grant PAPIIT IN119402 for partial support.

[29] Shadia Rifai Habbal thanks Tamitha L. Mulligan and another referee for their assistance in evaluating this paper.

References

Brueckner, G. E., J. P. Delaboudiniere, R. A. Howard, S. E. Paswaters, O. C. St. Cyr, R. Schwenn, P. L. Lamy, G. M. Simnett, B. Thompson, and D. Wang (1998), Geomagnetic storms caused by coronal mass ejections (CMEs): March 1996 through June 1997, *Geophys. Res. Lett.*, *25*, 3019.

Burlaga, L. F. (1995), *Interplanetary Magnetohydrodynamics*, Oxford Univ. Press, New York.

Burlaga, L. F., K. W. Behannon, and L. W. Klein (1987), Compound streams, magnetic clouds, and major geomagnetic storms, *J. Geophys. Res.*, *92*, 5725.

Burlaga, L. F., et al. (2001), Fast ejecta during the ascending phase of solar cycle 23: ACE observations, *J. Geophys. Res.*, *106*, 20,957.

Burlaga, L. F., S. P. Plunkett, and O. C. St. Cyr (2002), Compound streams, successive CMEs and complex ejecta, *J. Geophys. Res.*, *107*(A10), 1266, doi:10.1029/2001JA000255.

Burlaga, L., D. Berdichevsky, N. Gopalswamy, R. Lepping, and T. Zurbuchen (2003), Merged interaction regions at 1 AU, *J. Geophys. Res.*, *108*(A12), 1425, doi:10.1029/2003JA010088.

Burton, R. K., R. L. McPherron, and C. T. Russell (1975), An empirical relationship between interplanetary conditions and Dst, *J. Geophys. Res.*, *80*, 4204.

Cane, H. V., and I. G. Richardson (1997), What caused the large geomagnetic storm of November 1978?, *J. Geophys. Res.*, *120*, 17,445.

Cane, H. V., and I. G. Richardon (2003), Interplanetary coronal mass ejections in the near-Earth solar wind during 1996–2002, *J. Geophys. Res.*, *108*(A4), 1156, doi:10.1029/2002JA009817.

Cane, H. V., I. G. Richardson, and O. C. St. Cyr (2000), Coronal mass ejections, interplanetary ejecta and geomagnetic storms, *Geophys. Res. Lett.*, *27*, 3591.

Chen, M. W., L. R. Lyons, and M. Schulz (2000), Stormtime ring-current formation: A comparison between single-and double-dip model storms with similar transport characteristics, *J. Geophys. Res.*, *106*, 27,755.

Clua de Gonzalez, A. L., and W. D. Gonzalez (1998), Analytical study of the energy rate balance equation for the magnetospheric storm-ring current, *Ann. Geophys.*, *16*, 1445.

Crooker, N. U., J. T. Gosling, and S. W. Kahler (1998), Magnetic clouds at sector boundaries, *J. Geophys. Res.*, *103*, 301.

Daglis, I. A. (1997), The role of magnetosphere-ionosphere coupling in magnetic storm dynamics, in *Magnetic Storms*, *Geophys. Monogr. Ser.*, vol. 98, edited by B. T. Tsurutani et al., pp. 107, AGU, Washington, D. C.

Dasso, S., D. Gomez, and C. H. Mandrini (2002), Ring current decay rates of magnetic storms: a statistical study for 1957 to 1998, *J. Geophys. Res.*, *107*(A5), 1059, doi:10.1029/2000JA000430.

Fenimore, E. E. (1980), Solar wind flows associated with hot heavy ions, *Astrophys. J.*, *235*, 245.

Fenrich, F. R., and J. G. Luhmann (1998), Geomagnetic response to magnetic clouds of different polarity, *Geophys. Res. Lett.*, *25*, 2999.

Gloeckler, G., et al. (1999), Unusual composition of the solar wind in the 2–3 May 1998 CME observed with SWICS on ACE, *Geophys. Res. Lett.*, *26*, 157.

Gonzalez, W. D., J. A. Joselyn, Y. Kamide, H. W. Kroehl, G. Rostoker, B. T. Tsurutani, and V. M. Vasyliunas (1994), What is a geomagnetic storm?, *J. Geophys. Res.*, *99*, 5771.

Gonzalez, W. D., A. L. Clua de Gonzalez, J. H. A. Sobral, A. Dal Lago, and L. E. Vieira (2001), Solar and interplanetary causes of very intense geomagnetic storms, *J. Atmos. Terr. Phys.*, *63*, 403.

Gopalswamy, N. (2002), Relation between coronal mass ejections and their interplanetary counterparts, in *Solar-Terrestrial Magnetic Activity and Space Environment*, *COSPAR Colloq. Ser.*, vol. 14, edited by H. Wang and R. Xu, p. 157, Springer, New York.

Gopalswamy, N., A. Lara, R. P. Lepping, M. L. Kaiser, D. Berdichevsky, and O. C. St. Cyr (2000), Interplanetary acceleration of coronal mass ejections, *Geophys. Res. Lett.*, *27*, 145.

Gopalswamy, N., A. Lara, S. Yashiro, M. L. Kaiser, and R. A. Howard (2001), Predicting the 1-AU arrival times of coronal mass ejections, *J. Geophys. Res.*, *106*, 29,207.

Gopalswamy, N., S. Yashiro, G. Michalek, H. Xie, R. P. Lepping, and R. A. Howard (2005), Solar source of the largest geomagnetic storm of cycle 23, *Geophys. Res. Lett.*, *32*, L12S09, doi:10.1029/2004GL021639.

Grande, M., C. H. Perry, J. B. Blake, M. W. Chen, J. F. Fennell, and B. Wilken (1996), Observations of iron, silicon, and other heavy ions in the geostationary altitude region during late March 1991, *J. Geophys. Res.*, *101*, 24,707.

Hamilton, D. C., G. Gloeckler, F. M. Ipavich, B. Wilken, and W. Stuedemann (1988), Ring current development during the great geomagnetic storm of February 1986, *J. Geophys. Res.*, *93*, 14,343.

Henke, T., et al. (1998), Differences in the O^7/O^6 ratio in magnetic cloud and non-cloud coronal mass ejections, *Geophys. Res. Lett.*, *25*, 3465.

Kamide, Y., N. Yokoyama, W. Gonzalez, B. T. Tsurutani, I. A. Daglis, A. Brekke, and S. Masuda (1998), Two-step development of geomagnetic storms, *J. Geophys. Res.*, *103*, 6917.

Kozyra, J. U., J. E. Borovsky, M. W. Chen, M.-C. Fok, and V. K. Jordanova (1998), Plasma sheet preconditioning, enhanced convection and ring current development, in *Substorms-4*, edited by S. Kokubun and Y. Kamide, pp. 755–760, Terra Sci., Tokyo.

Kozyra, J. U., M. W. Liemohn, C. R. Clauer, A. J. Ridley, M. F. Thomsen, J. E. Borovsky, J. L. Roeder, V. K. Jordanova, and W. D. Gonzalez (2002), Multistep Dst development and ring current composition changes during the 4–6 June 1991 magnetic storm, *J. Geophys. Res.*, *107*(A8), 1224, doi:10.1029/2001JA000023.

Lepping, R. P., D. B. Berdichevsky, C.-C. Wu, A. Szabo, T. Narock, F. Mariani, A. J. Lazarus, and A. J. Quivers (2005), A summary of WIND magnetic clouds for the years 1995–2003: Model-fitted parameters, associated errors, and classifications, *Ann. Geophys.*, in press.

Lepri, S. T., T. H. Zurbuchen, L. A. Fisk, I. G. Richardson, H. V. Cane, and G. Gloeckler (2001), Fe charge distributions as an identifier of interplanetary coronal mass ejections, *J. Geophys. Res.*, *106*, 29,231.

Manoharan, P. K., N. Gopalswamy, S. Yashiro, A. Lara, G. Michalek, and R. A. Howard (2004), Influence of coronal mass ejection interaction on propagation of interplanetary shocks, *J. Geophys. Res.*, *109*, A06109, doi:10.1029/2003JA010300.

O'Brien, T. P., and R. L. McPherron (2000), An empirical phase space analysis of ring current dynamics: Solar wind control of injection and decay, *J. Geophys. Res.*, *105*, 7707.
Tsurutani, B. T., and W. D. Gonzalez (1997), The interplanetary causes of magnetic storms, in *Magnetic Storms*, *Geophys. Monogr. Ser.*, vol. 98, edited by B. T. Tsurutani et al., p. 77, AGU, Washington, D. C.
Wang, C. B., J. K. Chao, and C.-H. Lin (2003), Influence of the solar wind dynamic pressure on the decay and injection of the ring current, *J. Geophys. Res.*, *108*(A9), 1341, doi:10.1029/2003JA009851.
Wang, Y. M., P. Z. Ye, S. Wang, G. P. Zhou, and J. X. Wang (2002), Statistical study on the geoeffectiveness of Earth-directed coronal mass ejections from March 1997 to December 2000, *J. Geophys. Res.*, *107*(A11), 1340, doi:10.1029/2002JA009244.
Webb, D. F., E. W. Cliver, N. U. Crooker, O. C. St. Cry, and B. J. Thompson (2000), Relationship of halo coronal mass ejections, magnetic clouds, and magnetic storms, *J. Geophys. Res.*, *105*, 7491.
Xie, H., L. Ofman, and G. Lawrence (2004), Cone model for halo CMEs: Application to space weather forecasting, *J. Geophys. Res.*, *109*, A03109, doi:10.1029/2003JA010226.
Yashiro, S., N. Gopalswamy, G. Michalek, O. C. St.Cyr, S. P. Plunkett, N. B. Rich, and R. A. Howard (2004), A catalog of white light coronal mass ejections observed by the SOHO spacecraft, *J. Geophys. Res.*, *109*, A07105, doi:10.1029/2003JA010282.
Zhang, X., et al. (2003), Identification of solar sources of major geomagnetic storms between 1996 and 2000, *Astrophys. J.*, *582*, 520.

N. Gopalswamy, NASA Goddard Space Center, Code 695, Greenbelt, MD 20771, USA.

A. Lara, Instituto de Geofisica, National Autonomous University of Mexico, D.F. 04510 Mexico City, Mexico.

S. Lepri, Atmospheric, Oceanic, and Space Sciences, University of Michigan, 2455 Hayward Street, Ann Arbor, MI 48109, USA.

P. K. Manoharan, National Center for Radio Astronomy, Tata Institute of Fundamental Research, P. O. Box B, Udhagamandalam, Ooty 843 001, Tamilnadu, India.

H. Xie and S. Yashiro, Physics Department, Catholic University of America, 200 Hannan Hall, 640 Michigan Avenue NE, Washington, DC 20064, USA. (hong.xie@ssedmail.gsfc.nasa.gov)